Design and fabrication technology for high performance electrical pumped terahertz photonic crystal band edge lasers with complete photonic band gap

Hua Zhang (张华),[1,a)] Giacomo Scalari,[2] Jérôme Faist,[2] L. Andrea Dunbar,[1,b)] and Romuald Houdré[1,a)]
[1]*Institut de Physique de la Matière Condensée, Ecole Polytechnique Fédérale de Lausanne (EPFL), Station 3, Lausanne CH-1015, Switzerland*
[2]*Institut für Quantenelektronik, Eidgenössische Technische Hochschule Zürich (ETHZ), Zürich CH-8072, Switzerland*

(Received 25 April 2010; accepted 14 July 2010; published online 2 November 2010)

We detail the design and fabrication technology of two-dimensional photonic crystal (PhC) band edge emitting quantum cascade lasers (QCLs) operating at terahertz frequencies (~3.3 THz). The entire QCL active layer has been deeply etched to form a triangular lattice PhC, in which a complete in-plane photonic band gap for TM polarized light exists. Strong vertical optical confinement is provided by metal-metal plasmon waveguide fabricated with thermocompression bonding and planarization. Benzocyclobutene is employed as a low loss medium to planarize the PhC structure. By tailoring the top metal contact on the planarized PhC structures, electrical current injection pad can also be defined. The lasing properties can be controlled by engineering the photonic band structure. Broad band continuous single mode tuning over 30 GHz was observed; while lower current threshold density and higher operation temperature compared to Fabry–Perot (FP) asers were obtained. © *2010 American Institute of Physics*. [doi:10.1063/1.3476565]

I. INTRODUCTION

Photonic band engineering has been proved to be a very efficient way to tailor the emitting properties of semiconductor lasers. Thanks to the scaling law between wavelength (λ) and lattice constant (a), similar concepts of photonic crystal (PhC) semiconductor lasers can be exploited at any frequency.[1–7] For short wavelengths, e.g., UV range, visible range, and near-infrared, PhC structures commonly suffer from the subnanometer fabrication imperfections even with state of the art processing technique, challenging active and passive devices for practical applications. However, when the wavelength is scaled to longer wavelengths, e.g., far infrared or terahertz (THz) frequency, the corresponding critical dimensions required for the PhC devices are in the range of micrometers. Such large dimensions can be easily mastered through standard photolithography.

The recent demonstration of laser action in PhC quantum cascade lasers (QCLs) (Refs. 5–7) proved that PhC electromagnetic band and intersubband transitions engineering can be successfully combined to achieve high performance lasers. At THz frequencies, the structure of choice for the waveguide is the double plasmon (DP) scheme (or called metal-metal waveguide),[8] where the TM polarized light is confined in the active region between the two metallic layers. The DP metallic layers can also operate as electrical contacts. In contrast with PhC defect cavity lasers,[9] the core idea of this work is to use planar PhCs as two-dimensional (2D) distributed feedback (DFB) lasers.[10] In such case the lasers operate at the slow light band edge states or Van Hove singularities, where the low group velocity (v_g) and a large density of states are responsible for a significant gain enhancement, proportional to the product of the group index and the confinement of the field energy in the gain medium.[11–13]

Slow light PhC lasers can be achieved either with a high index modulation scheme or with a low index scheme, leading to strong PhC or weak PhC effects, respectively. Laser action based on weak PhC effect has been demonstrated with low index modulation structures that are obtained by patterning the top metallic layer of the laser[7,14] while leaving unetched the active region. The strong PhC effect, which requires high index modulation can be achieved with deeply etched structures[5,6,15] which are sandwiched within the two metallic layers, as illustrated in Figs. 1(a) and 1(b). The high index modulation scheme is quite attractive as the large band gap enables the localization of the laser mode over a smaller area than the one achieved by surface modulation by patterning the metal. Moreover, the periodical arrangement of active region material provides a better heat generation and dissipation distribution budget than the low index modulation case, as it allows a reduction in the active material and a better surface to volume ratio. Under the high index modulation scheme, pillar type PhC lasers are more appealing than the air hole type PhC lasers. One reason for this is that there are several complete photonic band gaps (PBGs) for the pillar type PhC for TM polarized light, another one is that the pillar type PhC lasers eliminate the risk of electrical leakage in contrast with PhC device with etched holes.[5,15]

In this paper, we focus on the design and fabrication

[a)]Electronic addresses: hua.zhang@epfl.ch, amd008@gmail.com, and romuald.houdre@epfl.ch.
[b)]Present address: Centre Suisse d'Electronique et de Microtechnique SA, Rue Jaquet-Droz 1, Neuchâtel, CH-2002, Switzerland.

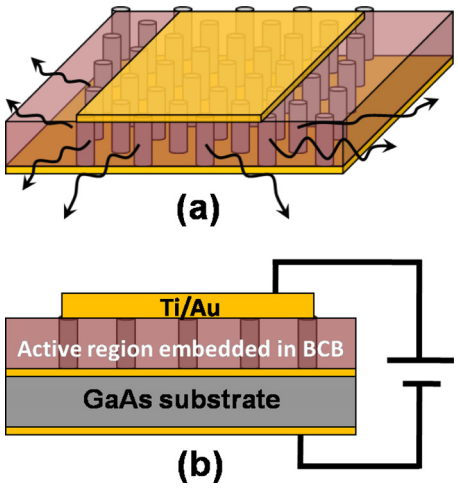

FIG. 1. (Color online) (a) Sketch of the lasing mode operation at the band edges corresponding to the in-plane emitting scheme. The pillar height is about 15 μm and the period range is between 14–23 μm. (b). Side view of the PhC QCL device.

technology aspects of electrically pumped QCLs with complete PBG. This paper first reviews the PhC dispersion band calculation and the photonic band parameters selection. It then details the fabrication process of pillar type PhC QCLs, with a multilayer Benzocyclobutene (BCB) planarization technique. Finally, it shows the high experimental performances of such pillar type PhC laser system regarding the threshold current density, maximum operation temperature, and single mode spectral control. In comparison to the high index contrast structure fabricated using a double wafer bonding techniques,[16] we believe our BCB planarization technique brings more freedom in terms of lithography, especially regarding the definition of the top contacts on these nonconnected structures.

II. DESIGN

The design of this PhC pillar type QCL has been systematically described in detail in our previous work,[6] so it will only be briefly summarized here. The plane wave expansion method[17] was used to model the planar PhC as a 2D system to calculate the in-plane band structure for TM polarized light. Figure 2 plots the calculated PhC dispersion band diagram calculated using real parts of the effective refractive indices of QCL ($n_{eff,QCL}=3.53$) and BCB ($n_{eff,BCB}=1.6$). There are several complete PBGs for this hexagonal/triangular pillar type PhC at different frequencies. The slow light regime, with flat-dispersion over a large k-vector range around high symmetry K and M points around the PBG1 is of particular interest. Such large k-vector states allow intrinsic in-plane emission. Note that the band edge states of PBG2 are located at $\Gamma=0$, which allow intrinsic emission in the direction normal to the sample surface.[18] Here we only focus on the PhC lasers operating at the PBG1 with in-plane emitting properties. Surface emitting structures will be reported separately elsewhere.[19]

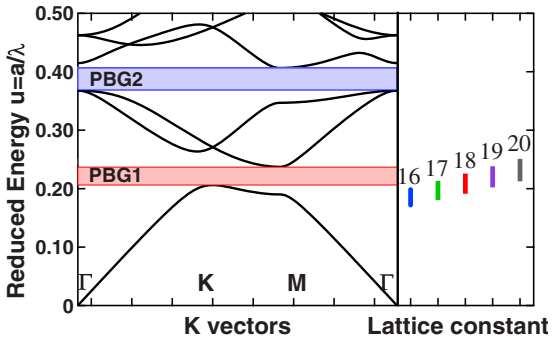

FIG. 2. (Color online) Superimposition of material gain bandwidth and PhC dispersion curves. Left panel shows PhC dispersion bands in reduced energy scale. Right panel shows the material gain bandwidth range in reduced energy scale for different lattice periods.

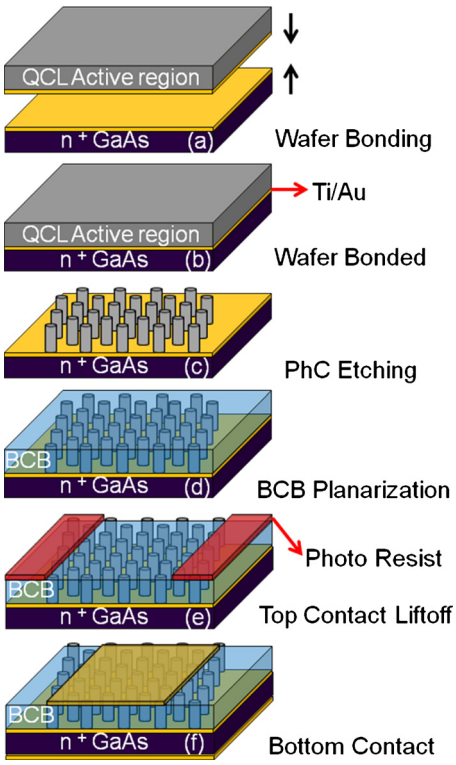

FIG. 3. (Color online) Complete fabrication flow chart of PhC pillar type QCLs.

In Fig. 2 the dispersion curves of the PhC structure and the QC material gain bandwidth (77 ~ 94 μm, 13.18 ~ 16.1 meV) are compared. The bandwidth for such intersubband transitions, is assumed to be identical to the spontaneous emission bandwidth. The pillar filling factor (ff) of the calculated PhC is 40%. All quantities are plotted in reduced units, $u=a/\lambda$ for the energy scale, and $k=k/(2\pi/a)$ for the wave vector. By scanning "a" from 14 to 23 μm (with 1 μm step size), the PBG1 can be fully covered.

III. FABRICATION TECHNOLOGY

The active layer used for the fabrication of PhC QCL consists of 120 periods of GaAs/$Al_{0.15}Ga_{0.85}As$, which is grown by molecular beam epitaxy on a semi-insulating GaAs substrate. Its energy band diagram investigated here is similar to that described in Ref. 20. A 700 nm thick $Al_{0.30}Ga_{0.70}As$ was grown as an etching stop layer. The flow chart shown in Fig. 3 illustrates the fabrication process steps

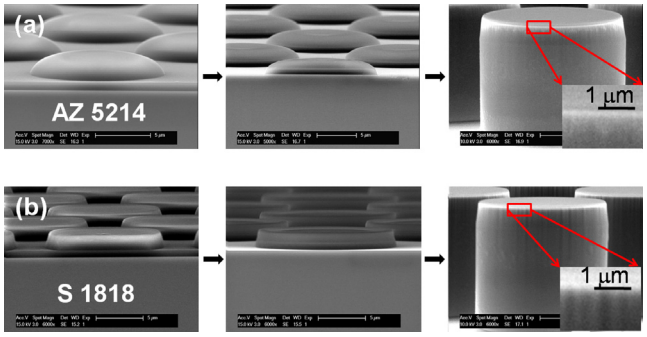

FIG. 4. (Color online) (a) Resist profile of AZ5214 (left), after SiO_2 mask transferring (middle), and after active region core etching (right). (b) Resist profile of S1818 (left), after SiO_2 mask transferring (middle), and after active region core etching (right).

for the pillar type PhC lasers based on above described QC active region. To create the metal-metal confinement, Ti/Au (5 nm/500 nm) layers were evaporated onto both the QCL structure and an n^+ doped substrate, the Au/Au surfaces of these wafers were then bonded together by means of thermocompression wafer bonding as illustrated in Fig. 3(a). This wafer-wafer bonding forms the first surface plasmon layer. It is performed in air at 300 °C with 4.5 MPa pressure for 45 min. Polishing of the substrate was performed, and then followed by the selective wet etching with a mixture solution containing citric acid [cirtic:H_2O_2:H_2O=3:2:3 in weight, Fig. 3(b)]. When the etch stop layer was reached, the sample was then processed with standard photolithography, reactive ion etching (RIE) was used to fabricate the pillars [Fig. 3(c)]. The structure was planarized using BCB [Fig. 3(d)]. A new metallic layer was deposited and lifted off [Fig. 3(e)] to form the second surface plasmon layer and the top contact as well. The bottom contact layer was formed by depositing metal on the n^+ GaAs substrate, as plotted in Fig. 3(f).

Detailed fabrication information after wafer bonding is given below: A 900 nm thick SiO_2 was deposited by plasma enhanced chemical vapor deposition (PECVD) on the epilayer, to form the hard mask for the following photolithography. In order to obtain smooth side wall profile of the pillar, it is necessary to obtain smooth hard mask profile. We used AZ5214 image reversal resist as a positive tone photoresist [Fig. 4(a)] to define the PhC pattern. The pattern was then transferred into the SiO_2 hard mask using a CHF_3/Ar based plasma mixture in RIE. The CHF_3/Ar plasma mixture with ratio of 25/25 [unit in SCCM (SCCM denotes cubic centimeter per minute at STP)] was used for the RIE step. The chamber pressure was kept at 30 mTorr with a radio frequency (rf) power of 200 W. Under such conditions, the etching rate is about 31 nm/min. A 29 min etching time is required to etch through the entire 900 nm SiO_2 layer. The reason to choose the image reversible photoresist AZ5214 rather than a positive resist such as S1818 [Fig. 4(b)] will be discussed and the results compared in detail. The key issue during the etching is that the in-plane roughness of the photoresist is more important than its vertical shape. During the first etching of SiO_2 hard mask, both AZ5214 and S1818 transfer almost the same angle to the SiO_2 hard mask [middle image in Figs. 4(a) and 4(b)]. However, the AZ5214 intrinsically transfers a much smoother in-plane profile to the SiO_2 layer than S1818, despite the vertical profile of AZ5214 resist that has a donut shape. This in-plane roughness on the SiO_2 introduced by the S1818 will be further amplified during the second etching, where the ~15.5 μm thick QCL active region is etched through. [Right hand side images in Figs. 4(a) and 4(b).] Detailed zooms on the edge of the pillars processed with the two resists are provided in the insert images. Such comparison demonstrates that the AZ5214 is the better choice for the SiO_2 mask etching.

After the first SiO_2 mask transfer, the sample was cleaned in warm acetone (40 °C) ultrasonic bath, and was then processed with oxygen plasma cleaning to remove the resist residue before the QCL core etching. For the second QCL active region etching, $SiCl_4$/Ar/Cl_2 plasma mixture with ratio of 46/6/1 (unit in SCCM) in the RIE was used. The chamber pressure was kept at 10 mTorr with a rf power of 100 W. Under such conditions, the etching rate is about 125 nm/min. A 120 min etching time is required to etch through the entire 15.5 μm active region. The PhC pillars after etching have almost 90° angle, with very smooth sidewall across the entire active region [right hand side image in Figs. 4(a) and 6(a)]. Such high quality etching leads to a considerable reduction in the propagation loss and scattering loss, and hence, it should effectively contribute to a lower threshold current density.

IV. MULTILAYER BCB PLANARIZATION

The biggest challenge in the fabrication of pillar type PhC QCL is to form the top plasmon/contact layer for the light confinement and uniform current injection purpose. Furthermore the planarization provides freedom on the definition of surface plasmon patterns, and potentially it forms a better heat-conducting environment surrounding the QCL material than air.[16] A multilayer planarization technique based on BCB (CYCLOTENE 3022–46) was applied to solve this issue. The BCB's low refractive index, low curing temperature, low loss, and ability to be dry etched are the most important features for this purpose. The standard single layer BCB planarization recipe, which suits for large piece wafer scale process, was modified with multilayer curing for small piece QCL devices. The single layer of thick BCB always results in much thicker resin at the edge than in the wafer center, this effect is critical when the BCB is coated on small device pieces. Moreover, one single layer coating of thick BCB cannot achieve smooth surface on 15.5 μm pillar after curing. An adhesive promoter (Dowing AP3000) was spin-coated on the sample before the first BCB layer to enhance the adhesion. The BCB was cured each time after the spin coating. N_2 purge is required when the curing temperature ramps higher than 180 °C to prevent the BCB oxidation.

Detailed curing information is plotted in Fig. 5. After three layers of spin coating and curing (two soft baking and one hard baking), the entire sample was completely covered with BCB with a smooth surface as seen in Fig. 6(b). The measured surface roughness is only ±28 nm, which is negligible comparing to the 15 μm total thickness. The BCB

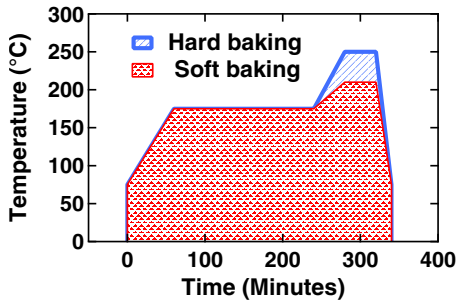

FIG. 5. (Color online) BCB curing information. Red: soft baking and blue: hard baking.

was etched without any surface preparation on the sample using a CF_4/O_2 plasma mixture with SCCM ratio of 40/60 in the RIE. The chamber pressure was kept at 100 mTorr with a rf power of 200 W. The BCB was etched to a depth a little bit lower than the top of the pillar, e.g., ~800 nm [Fig. 6(c)], in order to guarantee that the remaining SiO_2 mask can be easily removed through the following wet etching. The etching rate of the BCB strongly depends on the curing conditions; e.g., for a typical multilayer planarization process (two soft baking at 210 °C and one hard baking at 250 °C as shown in Fig. 5), the etching rate is 700 nm/min. This number can be slowed down to 370 nm/min in the case of a three hard baking curing process. When the BCB layer was ~800 nm over etched, i.e., below than the top of the pillar, the sample was then dipped in the buffered hydrofluoric acid to remove the remaining SiO_2 mask. Note that this step is very important because it determines the quality of the top metal contact; in another word it impacts on the laser current/voltage (IV) performance. A new pattern with negative photoresist TI35ES was written on the sample with ~4 μm thick undercut profile for thick metal contact lift-off. Very thick Ti/Au (5 nm/1200 nm) was evaporated on the device and then lifted off to generate a thick enough surface plasmon layer [Figs. 6(c)–6(f)], this thick layer compensates for the BCB over etching and surface roughness. The bottom contact was achieved by deposition of Ti/Au (5 nm/500 nm) on the bottom of the n^+ GaAs substrate. The sample was then cleaved and mounted on copper supporter with conductive glue and bonded with 25 μm gold wires [Figs. 6(g) and 6(h)].

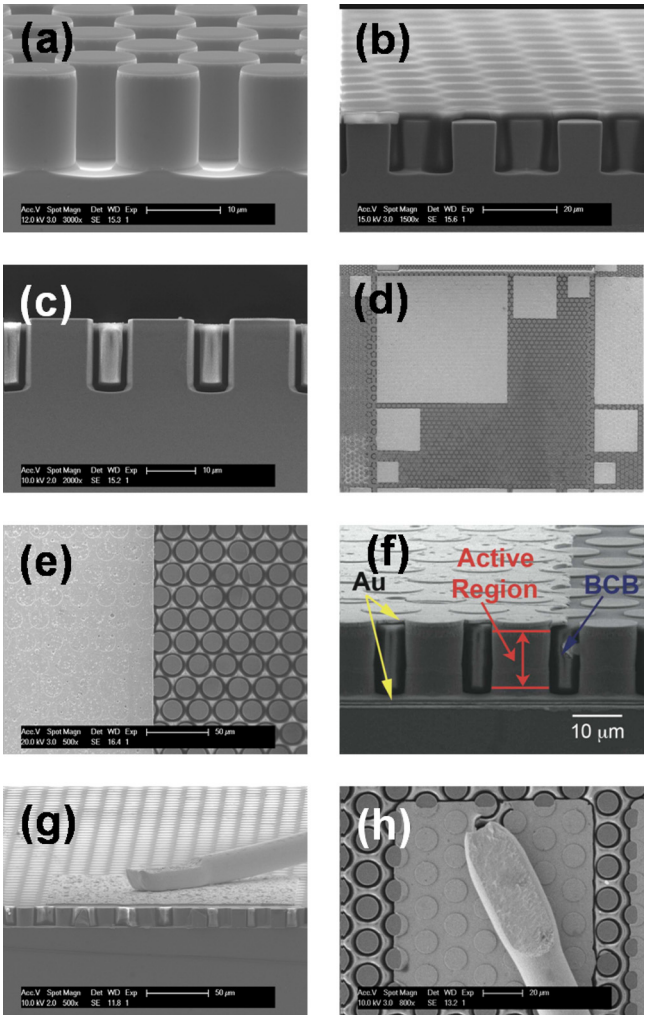

FIG. 6. (Color online) (a) Scanning electron microscopy (SEM) image of PhC pillars after RIE core etching. (b) Side view SEM image of the sample after multilayer BCB planarization. (c) Side view SEM image of the sample after BCB etching and SiO_2 removal. (d) SEM top view of metal contacts. (e) Detail of DP and single plasmon interface. (f) Side view of PhC pillars embedded in double metal waveguides with BCB filling material. (g) Side view of PhC pillar lasers after cleaving with bonding pad. (h) Top view of bonding pad on small contact (100×100 μm^2).

It is necessary to mention that such BCB planarization technique is not limited to the fabrication processes for pillar type TM polarized PhC QCL structures. It can be also used for more general purposes on various material systems where the device surfaces are intrinsically not smooth and require additional lithography, in e.g., PhC hole type structures with TE polarization, DFB lasers.

V. DEVICE CHARACTERIZATION

The lasing spectra characterizations and light-IV measurements were performed using a home-built, under-vacuum Fourier-transform-infrared spectrometer equipped with a He-cooled Si bolometer. Spectral measurements were performed with a step scan and lock-in technique. Figures 7(a) and 7(b) show the LIV measurements as a function of temperature for PhC lattice constants of $a=18$ μm and 17 μm, respectively. For $a=18$ μm, the lowest threshold current density of this laser is 120 A/cm^2 and the maximum operation temperature is 68 K. For $a=17$ μm, this PhC QCL laser operates up to 105 K under pulse condition. The current density starts to decay around 600 A/cm^2 for all the temperatures, such LI curve shape is caused by the energy mismatch between the material gain and the optical mode which limits the dynamic range. The $a=18$ μm PhC QC lasers shows narrower dynamic range, because with injection the gain spectrum is shifted into the PBG where no modes can exist.

To further investigate the improvement of temperature performance, we compare the threshold current density (J_{th}) versus temperature between PhC laser (600×600 μm^2), DP Fabry-Perot (FP) ridge laser (1170×100 μm^2), single plasmon FP ridge lasers (2000×200 μm^2) and microdisk laser (50 μm radius), as shown in Fig. 7(c). Note that all of these lasers were fabricated with the same active epilayer. Based

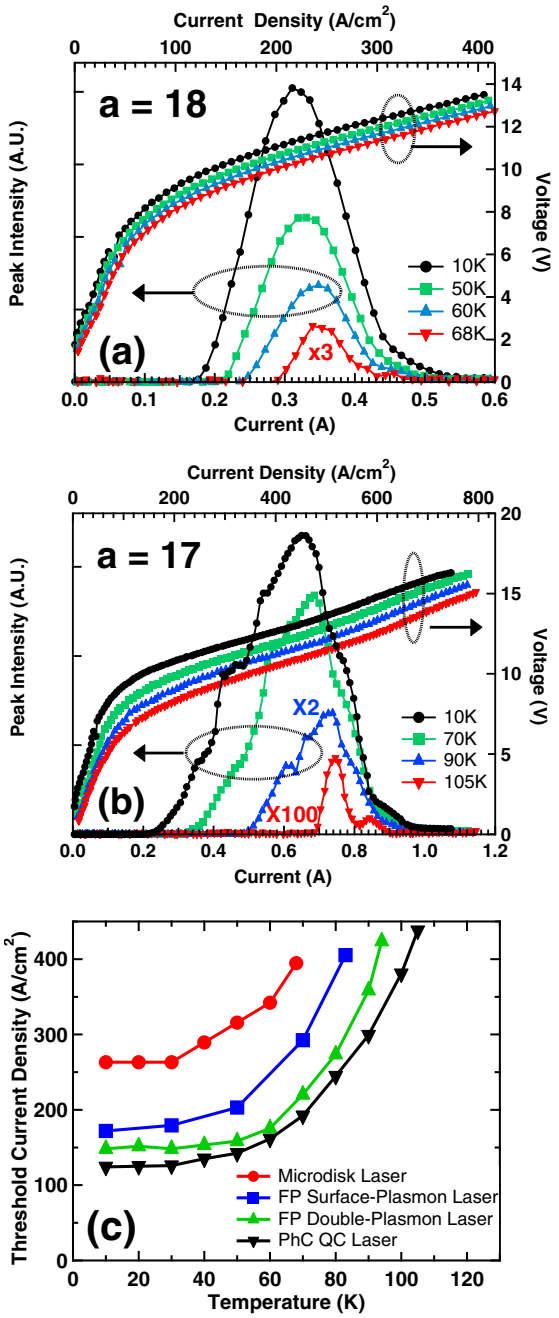

FIG. 7. (Color online) LIV characterization of THz QCL PhC lasers as a function of temperature and the comparison of maximum operation temperature between different material systems. (a) LIV characterization of peak intensity of the pillar type PhC laser at lattice parameter $a=18$ μm as a function of temperature under pulsed condition (pulse=200 ns, duty cycle =1.3%). The lowest threshold current density of this laser is 120 A/cm^2 and the maximum operation temperature is 68 K (intensity at 68 K has been scaled by a factor of 3). (b) LIV characterization of peak intensity of the pillar type PhC laser at lattice parameter $a=17$ μm as a function of temperature under pulsed condition (pulse=200 ns, duty cycle=1.3%). The lowest threshold current density of this laser is 128 A/cm^2 and the maximum operation temperature is 105 K (intensities at 90 and 105 K have been scaled by a factor of 2 and 100, respectively). (c) Comparison of maximum operation temperature between pillar type PhC laser(600×600 μm^2, red), DP FP ridge laser (1170×100 μm^2, green), surface plasmon FP ridge lasers (2000×200 μm^2, blue), and microdisk laser (50 μm radius, black). All devices are processed from the same epilayer.

on its lowest current threshold density, the pillar type PhC QCL has the highest operating temperature among all the waveguides we were able to realize, including the best DP

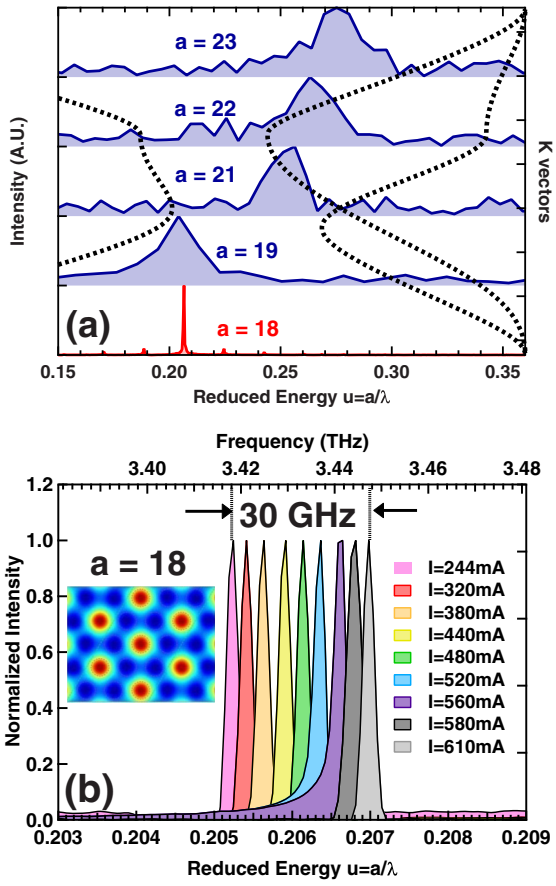

FIG. 8. (Color online) Spectra characterization of the PhC QC devices. (a) Comparison of EL (EL, shadow blue curves) and lasing spectra (shadow blue curve) at different lattice constants. When a $\leq$18 μm, the PhC devices are lasing. When a $\geq$19 μm, only EL single can be detected. Lasing spectra (solid curves) as a function of the injected current in continuous wave at a temperature of 25 K for a device of lattice constant $a=18$ μm at filling factor "ff" 40%. A 30 GHz continuously dynamic single mode tuning range is observed. Inset is the E_z field map of the corresponding PhC lasing state at band edge k point.

FP laser with very comparable injected current. This indicates that exploiting PhC band engineering can substantially enhance the gain and reduce the losses. The periodical pillar arrangement with BCB surrounding configuration provides a better heat generation and thermal dissipation scheme than the bulk counterparts, hence improves the temperature performance. The main advantage is that the gain (and consequently the heat generation) is only generated where it is useful, which scales as the ff of the structure. In addition there are two other favorable aspects, the first one is that the thermal generation is produced in a diluted medium (i.e., with a larger surface to volume ratio) and second the thermal conductivity of BCB (Ref. 21) is larger by a factor 10 compared to air.

VI. ELECTROLUMINESCENCE (EL) AND LASING MEASUREMENBT

Figure 8(a) shows the lasing or EL spectra of different lattice constants. Lasing behavior is observed when the lattice constants are smaller than 18 μm, this is because of the strong overlap between the material gain and the optical mode. When the lattice constants are larger than 18 μm,

only EL can be observed, this is because the frequency is either inside PBG or at air band (mode maximum in the air). This makes the optical mode cannot overlap with the material gain. The weak signals detected from in the spectra are the EL from the pillars in the sample boundary. Figure 8(b) shows the lasing spectra of the PhC QCL at lattice constant $a=18$ μm as a function of the injected current in continuous wave operation at a temperature of 25 K. Such frequency ($u \approx 0.206$) corresponds to the K band edge state referring to Fig. 2. As can be seen in Fig. 8(b), the single mode emission gradually shifts to higher energies by 30 GHz with increasing current density. Such tuning is achieved via increasing the injection current, and 30 GHz of continuous tuning counts for 0.81% of the wavelength. The cavity pulling effect and the field induced gain shift[22] allows such significant electrical tuning range.[6] This value is much higher than other types of devices based cavity pulling, such as FP lasers or microdisk lasers.[23] It is in a similar range compare to the result obtained by the less convenient temperature tuning experiments, e.g., DFB QCLs.[24] The E_z field map of the lasing K band edge state is shown as inset in Fig. 8.

VII. CONCLUSIONS

The design and fabrication technology of high performance pillar type PhC lasers based with THz QC active regions were reported. Multilayer BCB planarization technique was investigated to achieve DP confinement and current injection through each pillars. It is demonstrated that PhC laser is a promising candidate for THz QC light sources with enhancement on the key performances over known FP and microdisk lasers in all aspects. The pillar type PhC QCLs showed a substantial reduction in the threshold current density due to slow light effects. Highest operating temperature of the PhC laser among the others has been achieved. While remaining single mode, a significant electrical tuning over a frequency range of 30 GHz was achieved. It had been pointed out that one can achieve lasing action either in-plane or vertical direction using this technology. Based on the multilayer BCB planarization technique, the design and fabrication technology on band edge pillar type PhC QCL can bring a broad interest for the research and development on high performance optical pumping and electrical pumping light sources and detectors, or other various systems which require additional lithography on intrinsic nonsmooth surface.

ACKNOWLEDGMENTS

This work was supported by the Swiss National Science Foundation and the National Center of Competence in Research, Quantum Photonics.

[1] S. Riechel, C. Kallinger, U. Lemmer, J. Feldmann, A. Gombert, V. Wittwer, and U. Scherf, Appl. Phys. Lett. **77**, 2310 (2000).
[2] M. Scharrer, A. Yamilov, X. H. Wu, H. Cao, and R. P. H. Chang, Appl. Phys. Lett. **88**, 211103 (2006).
[3] M. Imada, S. Noda, A. Chutinan, T. Tokuda, M. Murata, and G. Sasaki, Appl. Phys. Lett. **75**, 316 (1999).
[4] A. Chen, S. J. Chua, G. C. Xing, W. Ji, X. H. Zhang, J. R. Dong, L. K. Jian, and E. A. Fitzgerald, Appl. Phys. Lett. **90**, 011113 (2007).
[5] R. Colombelli, K. Srinivasan, M. Troccoli, O. Painter, C. F. Gmachl, D. M. Tennant, A. M. Sergent, D. L. Sivco, A. Y. Cho, and F. Capasso, Science **302**, 1374 (2003).
[6] H. Zhang, L. A. Dunbar, G. Scalari, R. Houdré, and J. Faist, Opt. Express **15**, 16818 (2007).
[7] Y. Chassagneux, R. Colombelli, W. Maineult, S. Barbieri, H. E. Beere, D. A. Ritchie, S. P. Khanna, E. H. Linfield, and A. G. Davies, Nature (London) **457**, 174 (2009).
[8] B. S. Williams, S. Kumar, H. Callebaut, Q. Hu, and J. L. Reno, Appl. Phys. Lett. **83**, 2124 (2003).
[9] O. Painter, J. Vuckovic, and A. Scherer, J. Opt. Soc. Am. B **16**, 275 (1999).
[10] M. Meier, A. Mekis, A. Dodabalapur, A. Timko, R. E. Slusher, J. D. Joannopoulos, and O. Nalamasu, Appl. Phys. Lett. **74**, 7 (1999).
[11] J. P. Dowling, M. Scalora, M. J. Bloemer, and C. M. Bowden, J. Appl. Phys. **75**, 1896 (1994).
[12] S. Nojima, Jpn. J. Appl. Phys., Part 2 **37**, L565 (1998).
[13] S. Nojima, J. Appl. Phys. **90**, 545 (2001).
[14] L. Sirigu, R. Terazzi, M. I. Amanti, M. Giovannini, J. Faist, L. A. Dunbar, and R. Houdré, Opt. Express **16**, 5206 (2008).
[15] O. P. Marshall, V. Apostolopoulos, J. R. Freeman, R. Rungsawang, H. E. Beere, and D. A. Ritchie, Appl. Phys. Lett. **93**, 171112 (2008).
[16] A. Benz, C. Deutsch, G. Fasching, K. Unterrainer, A. M. Andrews, P. Klang, W. Schrenk, and G. Strasser, Opt. Express **17**, 941 (2009).
[17] M. Plihal and A. A. Maradudin, Phys. Rev. B **44**, 8565 (1991).
[18] H. Zhang, G. Scalari, R. Houdré, and J. Faist, European Conference on Lasers and Electro-Optics and the European Quantum Electronics Conference CLEO/Europe–EQEC, Munich, 2009, p. 5192585.
[19] H. Zhang, G. Scalari, R. Houdré, and J. Faist (unpublished).
[20] G. Scalari, N. Hoyler, M. Giovannini, and J. Faist, Appl. Phys. Lett. **86**, 181101 (2005).
[21] I. Christiaens, G. Roelkens, K. De Mesel, D. Van Thourhout, and R. Baets, J. Lightwave Technol. **23**, 517 (2005).
[22] A. Yariv, *Quantum Electronics*, 4 ed. (Saunders College Publishing, Philadelphia, 1991), Chap. 6, p. 181.
[23] L. A. Dunbar, R. Houdré, G. Scalari, L. Sirigu, M. Giovannini, and J. Faist, Appl. Phys. Lett. **90**, 141114 (2007).
[24] S. Kumar, B. S. Williams, Q. Qin, A. W. M. Lee, Q. Hu, and J. L. Reno, Opt. Express **15**, 113 (2007).